Geophysical Research Letters

RESEARCH LETTER
10.1029/2022GL101524

Key Points:

- The zonal and meridional momentum flux spectra exhibit a peak around the inertial period of 13 h in the troposphere (1.80–12.00 km)
- Height profiles of momentum flux, vertical wind power spectra, and kinetic energy display seasonal variation with a minimum during summer
- The maximum variability of momentum flux and vertical wind power spectra is noticed below tropopause and decreases with increasing height

Supporting Information:

Supporting Information may be found in the online version of this article.

Correspondence to:

P. Ghosh,
ghosh@iap-kborn.de

Citation:

Ghosh, P., Renkwitz, T., Latteck, R., Avsarkisov, V., & Chau, J. L. (2023). Momentum flux and vertical wind power spectral characteristics in the troposphere and lower stratosphere over Andøya, Norway as observed by MAARSY. *Geophysical Research Letters*, *50*, e2022GL101524. https://doi.org/10.1029/2022GL101524

Received 29 SEP 2022
Accepted 15 APR 2023

Author Contributions:

Conceptualization: Priyanka Ghosh, Jorge L. Chau
Data curation: Toralf Renkwitz, Ralph Latteck
Formal analysis: Priyanka Ghosh
Funding acquisition: Jorge L. Chau
Investigation: Priyanka Ghosh
Methodology: Priyanka Ghosh
Project Administration: Jorge L. Chau

Momentum Flux and Vertical Wind Power Spectral Characteristics in the Troposphere and Lower Stratosphere Over Andøya, Norway as Observed by MAARSY

Priyanka Ghosh[1], Toralf Renkwitz[1], Ralph Latteck[1], Victor Avsarkisov[1], and Jorge L. Chau[1]

[1]Leibniz-Institute of Atmospheric Physics at University of Rostock, Kühlungsborn, Germany

Abstract We used the tropospheric and lower stratospheric 3D winds for four consecutive years (2017–2020) to study the momentum flux (MF) and vertical wind power spectra (VWP) over Andøya, Norway (69.30°N, 16.04°E) using the Middle Atmosphere Alomar Radar System. The spectra range from 3.5 days$^{-1} > f >$ 30 min^{-1}, which are categorized in terms of observed/ground-based frequency (as the local inertial period is 13 h over Andøya), height ranges, and seasons. Our results indicate for the first time that (a) both the zonal and meridional MF display peaks around the inertial period (13 h) in the troposphere (1.80–12.00 km) during all seasons (with some exceptions), while VWP exhibits such features in the whole height range (1.80–18.00 km), (b) the minimum variability in MF, VWP, and kinetic energy is observed during summer, and (c) both the MF and VWP demonstrate height variation with maximum deviations below the tropopause.

Plain Language Summary The wind measurements are used to study the height and seasonal variation of momentum flux and vertical wind power spectra during 2017–2020. We report for the first time that both the momentum flux and vertical wind power spectra depict more variations in the tropospheric heights (around 1.80–7.20 km), below the tropopause, with the minimum amplitudes in the summer months (June–July–August). Moreover, long-period oscillations have more energy than short-period oscillations, and therefore, contribute more to the energy or flux transfer from the lower to the higher atmosphere. The month versus height profile of kinetic energy also portrays a similar feature with considerably more magnitude for the long-period oscillations than the short-period ones. The kinetic energy displays an enhancement of magnitude near the tropopause (~5.00–10.00 km).

1. Introduction

Atmospheric gravity waves (GWs) generated by various sources (topography, shear, and convection) mostly originate in the troposphere, transport momentum, and energy primarily in the vertical direction. Through their breaking and dissipation mechanism, the GWs deposit momentum in the mean field changing the general circulation of the middle atmosphere (Fritts & Alexander, 2003). The meridional flow generates a quasi-steady zonal flow to counter the Coriolis force, which is in turn supported by the wave-momentum transport in the region (Vincent & Reid, 1983). In the mesosphere, the momentum flux (MF) deposited by GWs acts as the dominant driving force of summer-to-winter pole material circulation and also reinforces the thermal structure of the atmosphere (e.g., Plumb, 2002). Although the dissipation of planetary waves can contribute to the quasi-steady flow, the internal GWs are considered to be the most important contributor to the momentum budget in the summer and winter hemispheres (e.g., Houghton, 1978).

The GWs, both orographic and non-orographic, propagate upwards in the atmosphere while interacting with the background winds. The general parameterization schemes of non-orographic GWs assume the sources of GWs to be nearly constant in the lower atmosphere (Alexander et al., 2010). Nevertheless, the GWs are not generated uniformly/continuously in the atmosphere. Lately, many studies reported that the individual GW packets portray an important role in the transportation and deposition of MFs rather than the continuous GWs, where the intermittent nature of GWs also plays a major role (Hertzog et al., 2008; Plougonven et al., 2013). Andrews et al. (1987) suggested that the sporadic GWs with large amplitudes are more likely to break at the lower heights depositing the momentum to the background atmosphere than the continuous GWs with smaller amplitudes and the same amount of mean MF. A mesosphere-stratosphere-troposphere (MST) radar offers an advantage to having a direct and accurate estimation of the MFs (e.g., Sato, 1994; Sato et al., 2017). The importance of GWs

Resources: Ralph Latteck, Jorge L. Chau
Software: Priyanka Ghosh, Ralph Latteck
Supervision: Jorge L. Chau
Validation: Priyanka Ghosh, Toralf Renkwitz
Visualization: Priyanka Ghosh
Writing – original draft: Priyanka Ghosh
Writing – review & editing: Priyanka Ghosh, Toralf Renkwitz, Ralph Latteck, Victor Avsarkisov, Jorge L. Chau

in the momentum budget in the stratosphere and mesosphere using the Middle and Upper Atmosphere (MU) radar (34.90°N, 136.10°E) was shown by Sato (1994) and Tsuda et al. (1990). By comparing the observations and model simulations (permitting GWs), Geller et al. (2013) found a significant bias in the GW source parameterization mostly in the polar regions.

In this paper, we present a statistical analysis of MF and vertical wind power (VWP) spectra using zonal, meridional, and vertical wind observations obtained by MAARSY in Andøya, Norway (69.30°N, 16.04°E). We focus on the stochastic nature of the observed periods for different seasons and height ranges, not on the statistics of deterministically identified waves. The paper is organized as follows. Section 2 describes briefly the radar instrument MAARSY and the analysis method used in this study. The characteristics of MF and VWP spectra during 2017–2020 are presented in Section 3. The possible mechanisms responsible for the observed MF and VWP spectra are discussed in Section 4, and the summary of our study is given in Section 5.

2. Data and Methodology

2.1. Instrument Details

We used the wind observations from the Middle Atmosphere Alomar Radar System (MAARSY), located in Andøya, Norway (69.30°N, 16.04°E), which is a monostatic radar operating at the frequency of 53.5 MHz with a maximum peak power of ∼866 kW. MAARSY comprises an active phased array with 433 individual circularly polarized Yagi antennas and an equal number of transceiver modules with individual phase control. The vertical and horizontal winds are obtained by a Doppler Beam Swinging experiment, measuring the radial velocity components for five beam pointing directions, vertical and four oblique beams into 10.5° zenith angle. MAARSY with its nearly circular layout leads to a symmetric radiation pattern with a half-power full beam-width of 3.6° (∼ 630 m at the height of 10 km). A comprehensive description of MAARSY was given in Latteck et al. (2010, 2012). MAARSY's monitor experiment is used for observing the troposphere and lower stratosphere from 2017 to 2020, covering the height ranges from 1.80 to 18.00 km. In this experiment, a single pulse and a 16-bit complementary coded pulse are subsequently used to improve the coverage for the middle troposphere as well as lower stratosphere and mesosphere, respectively. We have used the three-dimensional winds during the above-mentioned 48 months, including outlier rejection, with a temporal resolution of 15 min and an height resolution of 300 m. The minimum detectable wave period and vertical wavelength are 30 min and 600 m, respectively.

2.2. Analysis Method

We have followed the same analysis method as mentioned in Ghosh et al. (2022), whereby the wind data from the first 28 days of every month are split into four 7-day-wide windows, and the gaps shorter than 10 h are filled using a moving median. The zonal momentum flux (MF) spectra are calculated by multiplying the Fourier transform of zonal and vertical wind ($\mathcal{F}(u) \times \mathcal{F}(w)$) for each of the 7-day windows at every height after applying a Hanning window to inhibit the spectral leakage of the high-amplitude low-frequency fluctuations from contaminating the much weaker high-frequency spectral components. The obtained MF spectra for each of these 7-day windows are averaged to estimate the monthly MF. The monthly averaged MF spectra do not include missing data sets longer than 10 h. The meridional MF is also assessed in a similar method using the Fourier transform of the meridional and vertical wind ($\mathcal{F}(v) \times \mathcal{F}(w)$) along with the vertical wind power spectra ($\mathcal{F}(w) \times \mathcal{F}(w)$). The inertial frequency over Andøya is $\sim$ (13 h)$^{-1}$; therefore, we use this periodicity to discriminate between low- and high-frequency ranges. We have further categorized the monthly MF spectra in four height ranges, that is, 1.80–4.20 km (lower troposphere), 4.20–7.20 km (middle troposphere), 7.20–12.00 km (tropopause), and 12.00–18.00 km (lower stratosphere) to examine the height variation, and in terms of observed/ground-based frequency, that is, low- (>13 h) and high-frequency (<13 h) ranges. To study the seasonal variation of the MF spectra, they are categorized into four seasons: summer (JJA: June, July, August), autumn (SON: September, October, November), winter (DJF: December, January, February), and spring (MAM: March, April, May).

3. Results

3.1. Characteristics of Height Averaged Spectra

Figure 1 displays frequency versus MF spectra for zonal (a, d, g, j) and meridional (b, e, h, k) winds and VWP spectra (c, f, i, l) during autumn (September–November) from 2017 to 2020 at the heights of 1.80–18.00 km. The

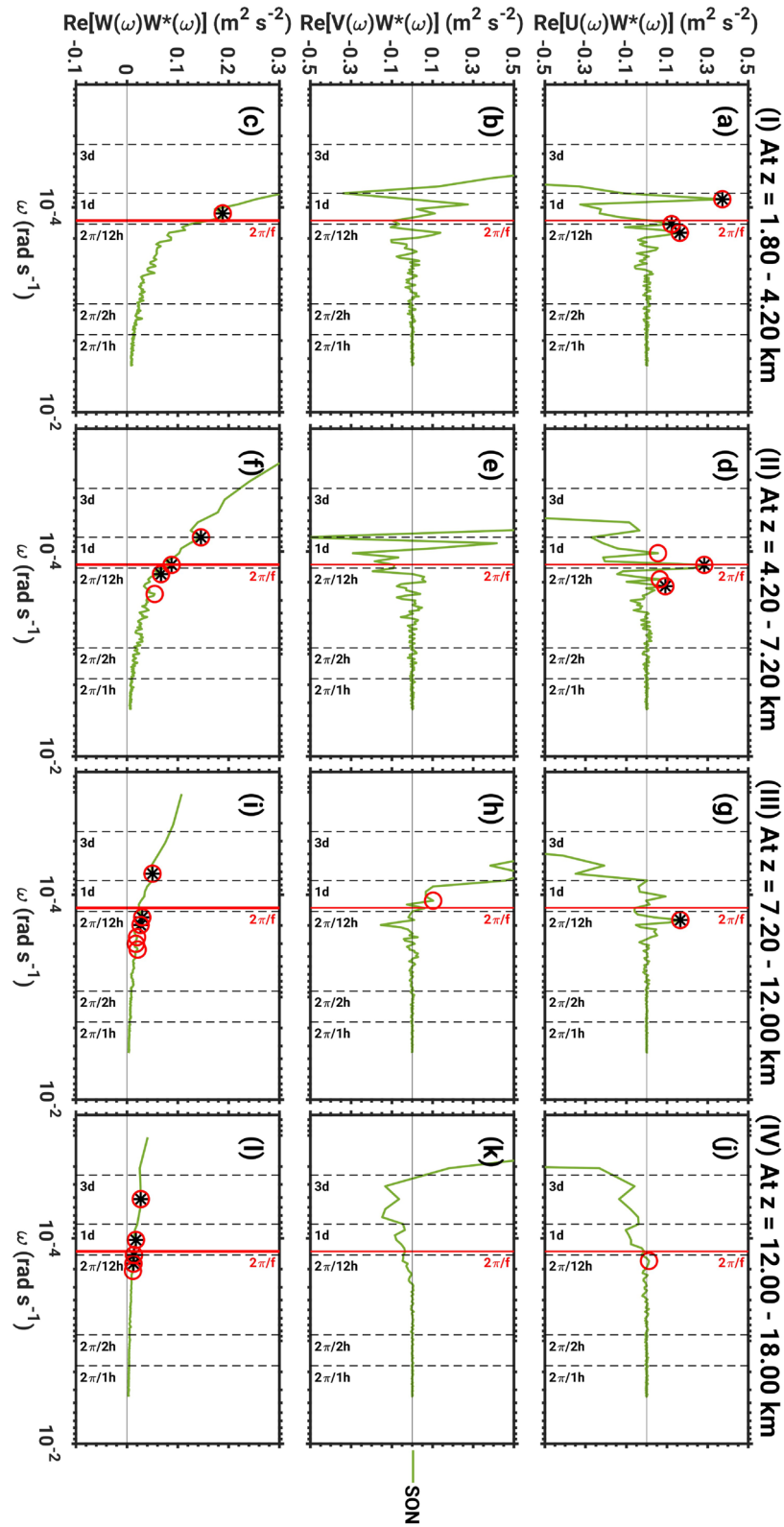

Figure 1. Frequency versus momentum flux spectra in the zonal (a), and meridional (b) direction, and vertical wind power spectra (c) averaged at heights of (i) z = 1.80–4.20 km in autumn (September–November, green line), during 2017–2020. The vertical red solid line indicates the inertial frequency ~ (13 h)$^{-1}$ at the radar site of Andøya (69.30°N). (d, e, f) is the same as (a, b, c) but at (II) z = 4.20–7.20 km, (g, h, i) at (III) z = 7.20–12.00 km, and (j, k, l) at (IV) z = 12.00–18.00 km. The red circles and black asterisks indicate peaks above 80% and 95% confidence level, respectively.

spectra are averaged for the height bins of 1.80–4.20 km, 4.20–7.20 km, 7.20–12.00 km, and 12.00–18.00 km. The peaks above 80% and 95% confidence level are marked with red circles and black asterisks, respectively. The spectra for winter, spring, and summer months are shown in Supporting Information S1 as Figures S1–S3, respectively. The wave-period ranging between 9–13 h is assumed to represent the near-inertial gravity waves (NIGWs), as the inertial period at the radar location is 13 h. Significant peaks are observed near inertial period in both zonal and meridional MF, mostly in the troposphere (1.80–12.00 km), indicating the dominance of NIGWs. The occurrence of peaks around 13 h varies seasonally, where significant peaks are not observed in meridional MF at 1.80–7.20 km during autumn. The confidence level for each height range varies such that the magnitude is larger in the lower troposphere than the upper stratosphere. Since the axes of Figure 1, Figures S1–S3 in Supporting Information S1 are kept similar to maintain uniformity, it gives an impression of a peak in the lower troposphere (1.80–7.20 km) for zonal and meridional MF. Some peaks are observed in the lower stratosphere (12.00–18.00 km) in zonal MF (during summer) and meridional MF (during winter and spring). It is also noted that the spectra flatten in the high-frequency range (<13 h, mainly below 6 h). Additionally, it is seen that meridional MF is mostly positive in the low-frequency range (above 1 day), while zonal MF is dominantly negative in the low-frequency range during most seasons. The amplitude of both zonal and meridional MFs is lower in summer (June–August, Figure S3 in Supporting Information S1). The values of more than 3 days are not considered in this study.

The frequency versus VWP spectra demonstrates significant peaks around inertial period in the whole height range during all seasons (bottom panel, Figure 1). Most of the significant peaks in the VWP correspond to the wave-period of 9–13 h (NIGWs). Although there are some exceptions, where significant peaks are observed beyond 1 day (at some height), they are not considered in our study (as it is beyond the scope of interest of the present paper). The VWP spectra are fairly smooth in the lower (1.80–4.20 km) and middle (4.20–7.20 km) tropospheric heights in the high-frequency range, while they are specifically flat in the upper troposphere and lower stratosphere (7.20–18.00 km). Most deviations are observed for the NIGWs scale (9–13 h) contributing predominantly to the energy spectrum. Interestingly, the magnitude of the VWP spectra decreases concerning height with the maximum magnitudes in the lower and middle troposphere, though the seasonal variation of the spectra is not apparent.

3.2. Attributes of Height Profile

Height profiles of the zonal (a, d, g, j) and meridional (b, e, h, k) MFs along with the VWP spectra (c, f, i, l) are portrayed in Figure 2 for the frequencies 30 min-2 h (I), 2–13 h (II), 13 h–1 day (III), and above 1 day (IV). Both zonal and meridional MFs exhibit maximum variation in the troposphere (∼1.80–7.20 km). The solid lines illustrate the median values, and the dotted lines on the left and right of the median indicate the 25-th and 75-th quartiles, respectively (in Figure 2). The deviations are determined as the distance between the solid and the dotted lines. The dominant MF direction is specified by the deviations in a particular direction for most of the height region in the height range of 1.80–18.00 km, whereby positive (negative) zonal MF indicates eastward (westward) and positive (negative) meridional MF denotes northward (southward) direction, respectively. It is perceived that the deviation of the MF decreases with the increasing height and the variation of MF is larger for 2–13 h ($\pm$0.001–0.003 $m^{-2}s^{-2}$) than 30 min-2 h ($\pm$0.02–0.05 $m^{-2}s^{-2}$) as depicted in Figures 2I and 2II. The MF reduces above 12.00 km for 2–13 h, indicating that the GWs could not propagate easily above 10.00 km height. For the shorter scales (30 min–2 h), there is a jump around 8.00–9.00 km demonstrated by the difference in the variability. Zonal MF is dominantly westward (i.e. negative) in the whole height (1.80–18.00 km). Meridional MF is largely northward (i.e. positive) in lower troposphere (below ∼7.00 km) except for autumn and above ∼7.00 km, and it becomes southward (i.e. negative). Moreover, the MF displays a seasonal variation with minimum during summer. Overall, it is observed that the variation is more in the lower troposphere than in the lower stratosphere.

The westward (i.e. negative) zonal MF becomes visible in low-frequencies as the deviation increases with the increasing time period, whereby it is around $\pm$0.50–1.00 $m^{-2}s^{-2}$ for 13 h–1 day [Figure 2(III)] and $\pm$15.00–30.00 $m^{-2}s^{-2}$ for the frequencies above 1 day [Figure 2(IV)]. Similar to Figures 2b and 2e), Figures 2h and 2k) also displays prominent northward (i.e. positive) meridional momentum flux in the whole height with the magnitude of $\pm$0.50–1.50 $m^{-2}s^{-2}$ and $\pm$10.00–30.00 $m^{-2}s^{-2}$ for 13 h to 1 day (Figure 2h) and above 1 day (Figure 2k), respectively, except for autumn (SON) of 13 h–1 day. It is observed that the variability of meridional MF is southward (i.e. negative) around 1.80–8.00 km and 11.00–18.00 km, while it is northward around

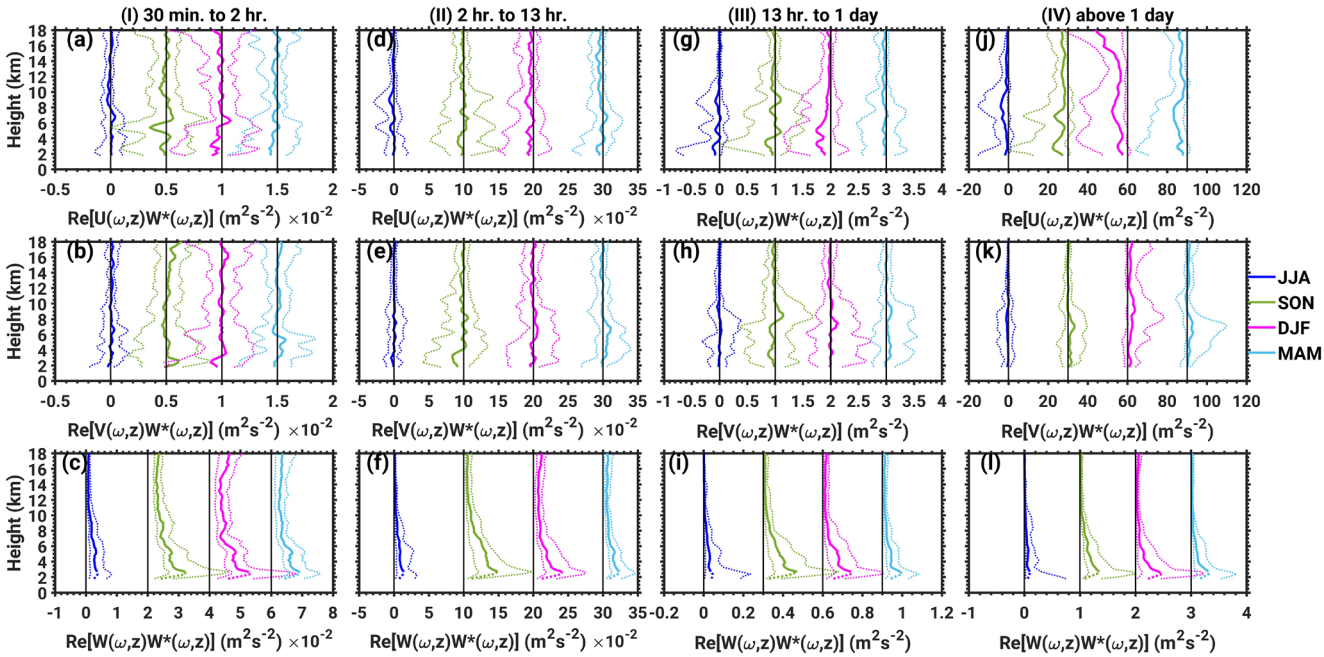

Figure 2. Height profile of zonal (a), and meridional (b) momentum fluxes, and vertical wind power spectra (c) for oscillations during 30 min–2 h (I). The different seasons are indicated with different color lines summer (blue), autumn (green), winter (magenta), and spring (cyan). The solid lines illustrate the median values and the dotted lines on the left and right of the median indicate the 25-th and 75-th quartiles, respectively. In panels (a) and (b), autumn is shifted by 0.005 $m^{-2}s^{-2}$, winter by 0.010 $m^{-2}s^{-2}$, and spring by 0.015 $m^{-2}s^{-2}$. In panel (c), autumn is shifted by 0.02 $m^{-2}s^{-2}$, winter by 0.04 $m^{-2}s^{-2}$, and spring by 0.06 $m^{-2}s^{-2}$. (d, e, f) is the same as (a, b, c) but for oscillations during 2–13 h (II). In panels (d), (e), and (f), autumn is shifted by 0.1 $m^{-2}s^{-2}$, winter by 0.2 $m^{-2}s^{-2}$, and spring by 0.3 $m^{-2}s^{-2}$. (g, h, i) is the same as (a, b, c) but for oscillations during 13 h–1 day (III). In panels (g), and (h), autumn is shifted by 1 $m^{-2}s^{-2}$, winter by 2 $m^{-2}s^{-2}$, and spring by 3 $m^{-2}s^{-2}$. In panel (i), autumn is shifted by 0.3 $m^{-2}s^{-2}$, winter by 0.6 $m^{-2}s^{-2}$, and spring by 0.9 $m^{-2}s^{-2}$. (j, k, l) is the same as (a, b, c) but for oscillations above 1 day (IV). In panels (j), and (k), autumn is shifted by 30 $m^{-2}s^{-2}$, winter by 60 $m^{-2}s^{-2}$, and spring by 90 $m^{-2}s^{-2}$. In panel (l), autumn is shifted by 1 $m^{-2}s^{-2}$, winter by 2 $m^{-2}s^{-2}$, and spring by 3 $m^{-2}s^{-2}$.

8.00–11.00 km. It is mostly southward for both zonal and meridional MF, except for meridional MF during 13 h–1 day (Figure 2h), where it behaves similarly to autumn. Both zonal and meridional MFs are weaker in summer similar to Figures 2b and 2e.

The height profile of VWP spectra is characterized by a height dependence, whereby the variation of VWP decreases corresponding to the increasing height. Analogous to the MF spectra, the deviation of VWP spectra also increases with an increasing period. The magnitude of VWP is ∼0.001–0.005 $m^{-2}s^{-2}$ for 30 min–2 h, ∼0.03–0.05 $m^{-2}s^{-2}$ for 2–13 h, ∼0.20–0.40 $m^{-2}s^{-2}$ for 13 h–1 day, and ∼0.50–0.80 $m^{-2}s^{-2}$ for above 1 day oscillations. A clear height dependence is evident for the height profiles of VWP spectra, where larger mean and variations are observed at lower heights. Moreover, the longer period oscillations (13 h–1 day and above 1 day) portray more magnitude in all the seasons than the smaller period oscillations (30 min–2 h and 2–13 h). It should be noted that the peak in the height profile of VWP ∼2–3 km is not considered for any interpretation as it could be due to measurement errors. Contamination of vertical winds by horizontal winds due to the finite half-power beam width (3.6°) during 2017–2020 was also checked in Ghosh et al. (2022). The correlation coefficient of ∼0.3–0.4 is observed between absolute horizontal winds versus absolute vertical winds (2017–2020), which is noticeable at lower heights. Nevertheless, this contamination decreases with increasing height (Figure S7 in Supporting Information S1, Ghosh et al. (2022)).

Month versus height profile of kinetic energy (KE) during 2017–2020 for the frequency ranges 30 min–2 h (a), 2–13 h (b), 13 h–1 day (c), and above 1 day (d) is shown in Figure 3. It is observed that KE varies concerning frequency, season, and height. The KE is less for 30 min–2 h (ranging between 0 and 3 Jkg^{-1}) than the other oscillations. The KE ranges between 0 and 6 Jkg^{-1} for 2–13 h and 13 h–1 day, while it is 0–50 Jkg^{-1} for above 1 day oscillations. Magnitude of KE increases as the wave-period increases, for example, 30 min–2 h < 2–13 h = 13 h–1 day < above 1 day. The magnitude of KE considerably increases at the heights of ∼5.00–10.00 km for all frequencies except for 30 min-2 h (at ∼5.00–8.00 km) where the magnitude increases slightly. Moreover, KE

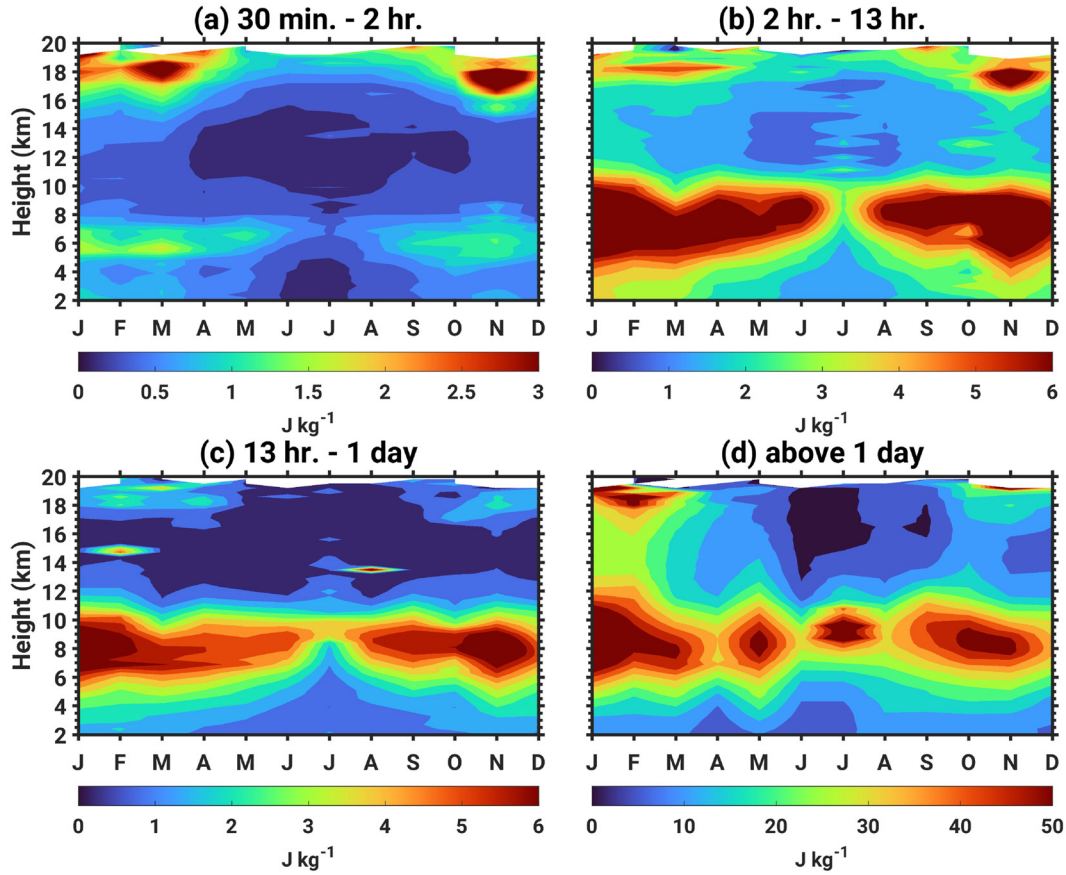

Figure 3. Month versus height profile of kinetic energy during 2017–2020 for the frequency ranges 30 min-2 h (a), 2–13 h (b), 13 h–1 day (c), and above 1 day (d) observed by the Middle Atmosphere Alomar Radar System over Andøya, Norway (69.30°N, 16.04°E).

exhibits seasonal variation with a minimum during summer (even at ∼5.00–10.00 km height) for 2–13 h and 13 h–1 day. Interestingly, the low-frequency oscillations above 1 day depict an increase of KE at ∼5.00–8.00 km during all months except for April, June, and August. Two peaks (maxima) are observed at the lower stratosphere (∼17.00–19.00 km) for all frequencies, but they are prominent for the high-frequency range (30 min–13 h).

4. Discussions

Using the three-dimensional wind measurements from MAARSY, the MF and VWP spectral characteristics during 2017–2020 are studied. We found that the height averaged MF spectra show significant peaks near the inertial period (13 h) in the troposphere, while peaks are observed in VWP spectra in both the troposphere and lower stratosphere. The height profile of MF and VWP spectra depicts deviation in magnitude concerning season, height, and wave period (or frequency range). The probable mechanisms responsible for such variations are discussed as follows.

4.1. Variation of MF and VWP Spectra in Troposphere and Stratosphere

Some observational studies on the frequency spectral characteristics of GWs in the troposphere and lower stratosphere indicated that the variances of GWs with near-inertial frequencies become dominant in the lower stratosphere, which is associated with a weak wind layer (Minamihara et al., 2018). Sato et al. (1997) studied the near-inertial period GWs characteristics using MU Radar in Shigaraki, Japan (34.90°N, 136.10°E), where the inertial period is 21 h and found that the 20 h period GWs dominated the stratosphere. According to Nastrom and Eaton (2006), the enhancement of wave energy around the inertial frequencies, especially strong during

summer in the stratosphere, is due to the decrease of energy with height in the lower frequencies, but the energy at the inertial frequency remains constant concerning height. This condition of constant energy with respect to the height near-inertial frequency suggests that any distant source would not affect the local wave refraction. Therefore, it is presumed that it can be only seen in the stratosphere during summer than in the winter months or in the troposphere (Nastrom & Eaton, 2006). However, in the present case, we observe a peak around the inertial period (∼13 h) in both the zonal and meridional MF spectra in the troposphere, though the magnitude of the peak is different during different seasons.

One fascinating feature is that the peak exists in the troposphere (1.80–12.00 km) but not in the lower stratospheric heights (12.00–18.00 km) unlike the previous studies. This does not correspond to the previous studies by Minamihara et al. (2018) and Nastrom and Eaton (2006). Nastrom et al. (1997) presumed that this enhancement of wave-activity at the near-inertial frequencies is due to the increase of kinetic energy versus potential energy. In our study, we found that the peak is more prominent in other seasons than in summer. It can be assumed that the wave activity near the inertial frequencies is considerably weaker in summer and the lower stratosphere (12.00–18.00 km). Another possible reason for the observed peak in the troposphere could be due to the influence of topography near MAARSY (Ghosh et al., 2022). Sato et al. (1999) found that vertical shear of the horizontal winds leads the higher-frequency wave components to presumably encounter critical levels above the westerly jet. We found the spectra in the high-frequency (<13 h) range nearly flat, which may be apparent due to the influence of the vertical shear of horizontal winds leading to critical level interactions. The composite mean zonal wind during 2017–2020 is ∼0–6 ms^{-1} below ∼8.00 km (Figure 2a; Ghosh et al. (2022)), corresponds to the very low magnitude of zonal winds in the lower troposphere, indicating critical-level filtering of orography generated waves at the radar site with nearly zero phase speed. The standard deviation in the zonal (meridional) wind is ∼0–9 ms^{-1} (∼±0–5 ms^{-1}) below 4.00 km and ∼10–15 ms^{-1} in both the zonal and meridional winds above 4.00 km [Figures 2d and 2e; Ghosh et al. (2022)]. Our observation of peaks in the MF spectra in the troposphere could be due to the variations in the background wind and the buoyancy frequency (modulated by the wave thermodynamics) for the gravity waves crossing the tropopause or frontal systems (Wei & Zhang, 2015).

The VWP spectra show significant peaks (above 95% confidence level) around the inertial period during all seasons and in the whole height range of 1.80–18.00 km. Most of the significant peaks in the VWP correspond to the wave-period of NIGWs (9–13 h), although there are some exceptions when a significant peak is observed beyond 1 day (not considered in this study). The standard deviation of the composite vertical wind is 0.15–0.25 ms^{-1} around the tropopause heights, which is much smaller than the standard deviation of the horizontal winds at that same height. Moreover, the composite mean of vertical wind during 2017–2020 ranges between ±0.05 ms^{-1} in the whole height profile of 1.80–18.00 km. The different behavior of VWP could be because the background conditions are less affected as the vertical wind has comparatively lesser magnitude than the horizontal winds. Using ray-tracing technique, Wang et al. (2009) found that the propagating environment considerably affects the propagation characteristics of waves, where the waves exhibit strong variations, mainly in the horizontal direction. This further supports our observation. It can be assumed that the peak in the troposphere is due to the contribution of the inertial period (∼13 h) along with NIGWs, which is mostly absent in the stratosphere owing to the existence of the weak wind layer (Minamihara et al., 2018).

4.2. Dependence of MF and VWP Spectra on Frequency and Season

Minamihara et al. (2016) studied the VWP using PANSY (Program of the Antarctic Syowa MST/IS) radar observations over Syowa Station (69.01°S, 39.59°E), Antarctic, and found that the magnitude of VWP is larger for the short-period components ($\tau < 2$ h). Our study reports that the deviation of magnitude is more for the long-period components than the short-period components. Sato et al. (2017) found that the zonal MF spectra are mainly positive while the meridional MF spectra are mostly negative in the mesosphere (84–88 km), using PANSY in Antarctic observations during Polar Mesospheric Summer Echoes over 3 years. They suggested that the GWs propagate in the eastward and poleward direction dominantly concerning the mean wind indicating the transfer of energy to the mesosphere by the GWs generated in the lower atmosphere. Since the zonal MF spectra are mostly negative, and the meridional MF is dominantly positive in the present study, it can be assumed that the GWs in the troposphere and lower stratosphere are largely westward and poleward directions around the MAARSY location. The probable reason could be the geographically conjugate location of PANSY (69.01°S, 39.59°E) and MAARSY (69.30°N, 16.04°E) influencing the direction of propagation of GWs as they both are located at nearly

the same latitudes but in different hemispheres. This could also indicate the probable interhemispheric coupling of waves, which needs further investigation. Sato et al. (1999) noted that the NIGWs have a nearly horizontal component vector, which leads to the propagation of GWs to poleward latitudes based on their location (using a global circulation model). Our observation of positive meridional MF indicating poleward propagation of GWs matches well with the findings of Sato et al. (1999).

Several studies in the past suggest that convection is an excitation mechanism for low-frequency GWs, which is enhanced during the summer months (Riggin et al., 2002; Sato et al., 2003). Nastrom and Eaton (2006) explained the seasonal variation of the quasi-monochromatic oscillation by the percent of wind variance and found about 50% cases in the stratosphere showed the existence of quasi-monochromatic oscillation during summer. We observed that both the zonal and meridional MF and VWP spectra exhibit seasonal variation with minimum deviation during the summer months. Nastrom et al. (1997) found that the ratio of stratospheric to tropospheric spectral amplitudes is considerably smaller than the predicted amplitude without any attenuation in the troposphere and stratosphere. They suggested that the wave energy in the troposphere gets attenuated around 85%–90% during the GWs propagation from the troposphere to the stratosphere. This could be due to the reflection or absorption GWs in this region, and it also indicates that the GWs sources are principally in or below the tropospheric segment (Nastrom et al., 1997). Corresponding enhancements are visible at such heights in our month versus KE height profile (Figures 3b and 3c). The additional peaks in KE (mainly below 13 h) at lower stratospheric heights (∼17.00–19.00 km) could be the impact of the secondary GWs generation at tropopause during January–April and October–December. In our study, we observed the variation in the height profile of MF (both zonal and meridional) and VWP spectra with the maximum deviation in the tropospheric heights (∼1.80–7.20 km). The deviation relatively decreases at the tropopause and lower stratospheric heights (∼7.20–18.00 km). This height dependence of the deviation/variation of MF and VWP spectra could be presumably because GWs are dominantly generated in the troposphere or due to enhanced attenuation of GWs in the troposphere.

Some studies found that the directional momentum flux estimated using a statistical approach along with the Helmholtz decomposition technique (separating the divergent and rotational components of the winds) is a robust technique, using either aircraft and ship-based observation or high-resolution global circulation model (Callies et al., 2016; Wei et al., 2022). We need to have measurements with spatial coverage in the horizontal direction to implement the decomposition technique. The present configuration of MAARSY provides wind measurements at a particular location. However, it is possible to implement this decomposition technique with MAARSY 3D measurements in the future. Since MAARSY is located at 69.30°N, it can be assumed that convection may not be a dominant GWs source mechanism, instead, orography and wind shear could be. Evidence of noisiness can be seen in the lower troposphere during autumn and winter, around 2.00–6.00 km heights (Figures 2c, f, i, and l), while it is not visible in spring and summer. Concerning the gross underestimation in the directional momentum flux spectra, no large discrepancy is evident in these spectra for different oscillation periods. This can be interpreted as a certain degree of consistency in our results needing more extensive study. The same is valid for the influence of boundary layer, shallow convection (Stephan et al., 2020), wind shear, and orography.

5. Summary and Conclusions

In the present work, we studied the height and seasonal variation of MF (zonal and meridional) and VWP spectra in the troposphere and lower stratosphere (1.80–18.00 km) during 2017–2020 over Andøya, Norway (69.30°N, 16.04°E) using MAARSY. The MF and VWP spectra are categorized in terms of the frequency range, averaged height over specific height regions and seasons to study the statistical characteristics of seasonal and height variation. The important outcomes from our study, which we report for the first time (best to our knowledge), are as follows.

1. Height averaged spectral characteristics: The height averaged zonal and meridional MF spectra exhibit a peak around the inertial period (∼13 h) in the troposphere with seasonal variations, which could be due to the effect of the NIGWs. Although there are some small peaks in the low-frequency range (>13 h), the high-frequency range (<13 h) appears quite flat. The height averaged VWP spectra display a peak near the tropopause and lower stratospheric heights (7.20–18.00 km) but the spectra in the low-frequency range are comparatively flatter than the MF spectra.
2. Height profile spectral characteristics: The height profile of both the zonal and meridional MF spectra display seasonal and height variation with minimum MF in the summer months (JJA) and maximum deviation below

~8–10 km height. Another interesting feature noticed is that the magnitude of the deviation decreases with increasing height. The height profile of VWP spectra also depicts similar height and seasonal variations. The enhancement of the deviation of VWP below ~3 km could be due to measurement errors and is not considered for any interpretation. It is also noticed that the magnitude of deviation for both MF and VWP increases with increasing periods indicating that the low-frequency components contribute more to the MF and VWP rather than the high-frequency components. The month versus height profile of KE also depicts variation with height with the maximum magnitude at ~5.00–10.00 km for all frequencies, suggesting the possible reflection/absorption of the GWs generated in the troposphere. The KE varies seasonally with a minimum during summer except for the period above 1 day similar to the MF spectra indicating the probable low GWs activity at the radar location. Additionally, two peaks are observed in the KE in the lower stratosphere (~17.00–19.00 km) during January–April and October–December, indicating the possible secondary GWs generation at the tropopause.

Therefore, the present study gives a detailed synopsis of the MF and VWP spectra in the troposphere and lower stratosphere over Northern Norway using the wind observations from MAARSY, which could probably be used to improve the parameterization schemes of global circulation models near the polar latitudes. Although our preliminary results might represent the combination of divergent and rotational wind components, we plan to improve multistatic observations in the future to separate their contributions.

Data Availability Statement

The data supporting this study is available at https://doi.org/10.22000/766.

Acknowledgments
Priyanka Ghosh would like to thank Maosheng He for the fruitful discussions. This research has been supported by DFG (VACILT, Grant PO 2341/2-1) and BMBF (TIMA in the frame of ROMIC, Grant 01 LG 1902A). We are grateful to the reviewers for their insightful suggestions. Open Access funding enabled and organized by Projekt DEAL.

References

Alexander, M. J., Geller, M., McLandress, C., Polavarapu, S., Preusse, P., Sassi, F., et al. (2010). Recent developments in gravity-wave effects in climate models and the global distribution of gravity-wave momentum flux from observations and models. *Quarterly Journal of the Royal Meteorological Society*, *136*(650), 1103–1124. https://doi.org/10.1002/qj.637

Andrews, D. G., Holton, J. R., & Leovy, C. B. (1987). *Middle atmosphere dynamics* (Vol. 40, p. 1–489). Academic Press.

Callies, J., Bühler, O., & Ferrari, R. (2016). The dynamics of mesoscale winds in the upper troposphere and lower stratosphere. *Journal of the Atmospheric Sciences*, *73*(12), 4853–4872. https://doi.org/10.1175/JAS-D-16-0108.1

Fritts, D. C., & Alexander, M. J. (2003). Gravity wave dynamics and effects in the middle atmosphere. *Reviews of Geophysics*, *41*(1). https://doi.org/10.1029/2001RG000106

Geller, M. A., Alexander, M. J., Love, P. T., Bacmeister, J., Ern, M., Hertzog, A., et al. (2013). A comparison between gravity wave momentum fluxes in observations and climate models. *Journal of Climate*, *26*(17), 6383–6405. https://doi.org/10.1175/JCLI-D-12-00545.1

Ghosh, P., He, M., Latteck, R., Renkwitz, T., Avsarkisov, V., Zecha, M., & Chau, J. L. (2022). Characteristics of frequency-power spectra in the troposphere and lower stratosphere over andøya (Norway) revealed by MAARSY. *Journal of Geophysical Research: Atmospheres*, *127*(13), e2021JD036343. https://doi.org/10.1029/2021JD036343

Hertzog, A., Boccara, G., Vincent, R. A., Vial, F., & Cocquerez, P. (2008). On the relation between gravity waves and wind speed in the lower stratosphere over the southern ocean. *Journal of the Atmospheric Sciences*, *65*(10), 3056–3070. https://doi.org/10.1175/2008JAS2710.1

Houghton, J. T. (1978). The stratosphere and mesosphere. *Quarterly Journal of the Royal Meteorological Society*, *104*(439), 1–29. https://doi.org/10.1002/qj.49710443902

Latteck, R., Singer, W., Rapp, M., & Renkwitz, T. (2010). Maarsy – The new MST radar on andøya/Norway. *Advances in Radio Science*, *8*, 219–224. https://doi.org/10.5194/ars-8-219-2010

Latteck, R., Singer, W., Rapp, M., Vandepeer, B., Renkwitz, T., Zecha, M., & Stober, G. (2012). MAARSY: The new MST radar on andøya—System description and first results. *Radio Science*, *47*(1). https://doi.org/10.1029/2011RS004775

Minamihara, Y., Sato, K., Kohma, M., & Tsutsumi, M. (2016). Characteristics of vertical wind fluctuations in the lower troposphere at Syowa station in the Antarctic revealed by the pansy radar. *SOLA*, *12*(0), 116–120. https://doi.org/10.2151/sola.2016-026

Minamihara, Y., Sato, K., Tsutsumi, M., & Sato, T. (2018). Statistical characteristics of gravity waves with near-inertial frequencies in the Antarctic troposphere and lower stratosphere observed by the pansy radar. *Journal of Geophysical Research: Atmospheres*, *123*(17), 8993–9010. https://doi.org/10.1029/2017JD028128

Nastrom, G. D., & Eaton, F. D. (2006). Quasi-monochromatic inertia-gravity waves in the lower stratosphere from MST radar observations. *Journal of Geophysical Research: Atmospheres*, *111*(D19), D19103. https://doi.org/10.1029/2006JD007335

Nastrom, G. D., Van Zandt, T. E., & Warnock, J. M. (1997). Vertical wavenumber spectra of wind and temperature from high-resolution balloon soundings over Illinois. *Journal of Geophysical Research: Atmospheres*, *102*(D6), 6685–6701. https://doi.org/10.1029/96JD03784

Plougonven, R., Hertzog, A., & Guez, L. (2013). Gravity waves over Antarctica and the southern ocean: Consistent momentum fluxes in mesoscale simulations and stratospheric balloon observations. *Quarterly Journal of the Royal Meteorological Society*, *139*(670), 101–118. https://doi.org/10.1002/qj.1965

Plumb, R. A. (2002). Stratospheric transport. *Journal of the Meteorological Society of Japan Series II*, *80*(4B), 793–809. https://doi.org/10.2151/jmsj.80.793

Riggin, D. M., Kudeki, E., Feng, Z., Sarango, M. F., & Lieberman, R. S. (2002). Jicamarca radar observations of the diurnal and semidiurnal tide in the troposphere and lower stratosphere. *Journal of Geophysical Research: Atmospheres*, *107*(D8), 4062. https://doi.org/10.1029/2001JD001216

Sato, K. (1994). A statistical study of the structure, saturation and sources of inertio-gravity waves in the lower stratosphere observed with the MU radar. *Journal of Atmospheric and Terrestrial Physics*, *56*(6), 755–774. https://doi.org/10.1016/0021-9169(94)90131-7

Sato, K., Kohma, M., Tsutsumi, M., & Sato, T. (2017). Frequency spectra and vertical profiles of wind fluctuations in the summer Antarctic mesosphere revealed by MST radar observations. *Journal of Geophysical Research: Atmospheres*, *122*(1), 3–19. https://doi.org/10.1002/2016JD025834

Sato, K., Kumakura, T., & Takahashi, M. (1999). Gravity waves appearing in a high-resolution GCM simulation. *Journal of the Atmospheric Sciences*, *56*(8), 1005–1018. https://doi.org/10.1175/1520-0469(1999)056⟨1005:GWAIAH⟩2.0.CO;2

Sato, K., O'Sullivan, D. J., & Dunkerton, T. J. (1997). Low-frequency inertia-gravity waves in the stratosphere revealed by three-week continuous observation with the MU radar. *Geophysical Research Letters*, *24*(14), 1739–1742. https://doi.org/10.1029/97GL01759

Sato, K., Yamamori, M., Ogino, S.-Y., Takahashi, N., Tomikawa, Y., & Yamanouchi, T. (2003). A meridional scan of the stratospheric gravity wave field over the ocean in 2001 (MESSO2001). *Journal of Geophysical Research: Atmospheres*, *108*(D16), ACL3-1–ACL3-13. https://doi.org/10.1029/2002JD003219

Stephan, C. C., Lane, T. P., & Jakob, C. (2020). Gravity wave influences on mesoscale divergence: An observational case study. *Geophysical Research Letters*, *47*(1), e2019GL086539. https://doi.org/10.1029/2019GL086539

Tsuda, T., Murayama, Y., Yamamoto, M., Kato, S., & Fukao, S. (1990). Seasonal variation of momentum flux in the mesosphere observed with the MU radar. *Geophysical Research Letters*, *17*(6), 725–728. https://doi.org/10.1029/GL017i006p00725

Vincent, R. A., & Reid, I. M. (1983). Hf Doppler measurements of mesospheric gravity wave momentum fluxes. *Journal of the Atmospheric Sciences*, *40*(5), 1321–1333. https://doi.org/10.1175/1520-0469(1983)040⟨1321:HDMOMG⟩2.0.CO;2

Wang, S., Zhang, F., & Snyder, C. (2009). Generation and propagation of inertia–gravity waves from vortex dipoles and jets. *Journal of the Atmospheric Sciences*, *66*(5), 1294–1314. https://doi.org/10.1175/2008JAS2830.1

Wei, J., & Zhang, F. (2015). Tracking gravity waves in moist baroclinic jet-front systems. *Journal of Advances in Modeling Earth Systems*, *7*(1), 67–91. https://doi.org/10.1002/2014MS000395

Wei, J., Zhang, F., Richter, J. H., Alexander, M. J., & Sun, Y. Q. (2022). Global distributions of tropospheric and stratospheric gravity wave momentum fluxes resolved by the 9-km ECMWF experiments. *Journal of the Atmospheric Sciences*, *79*(10), 2621–2644. https://doi.org/10.1175/JAS-D-21-0173.1